LI-RADS v2018 major criteria: Do hepatocellular carcinomas in non-alcoholic steatohepatitis differ from those in virus-induced chronic liver disease on MRI?

Maxime Barat, Thi Thuy Linh Nguyen, Clémence Hollande, Jean-Baptiste Coty, Christine Hoeffel, Benoit Terris, Anthony Dohan, Vincent Mallet, Stanislas Pol, Philippe Soyer

Version of Record: https://www.sciencedirect.com/science/article/pii/S0720048X21001315
Manuscript_2f1cb5b1a4e79a25a344fa9e036e2576

Original article

LI-RADS v2018 major criteria: do hepatocellular carcinomas in non-alcoholic steatohepatitis differ from those in virus-induced chronic liver disease on MRI?

Authors

Maxime BARAT [a, b*]

Thi Thuy Linh NGUYEN [a, c]

Clémence HOLLANDE [b, d]

Jean-Baptiste COTY [a, b]

Christine HOEFFEL [e]

Benoit TERRIS [b, f]

Anthony DOHAN [a, b]

Vincent MALLET [b, d]

Stanislas POL [b, d]

Philippe SOYER [a,b]

Affiliations

[a] Department of Radiology, Hôpital Cochin, Assistance Publique-Hôpitaux de Paris, 75014 Paris, France

[b] Université de Paris, 75006 Paris, France

[c] Department of Radiology, Hue University of Medicine and Pharmacy, Hue University, Hue City 530000, Vietnam

[d] Department of Hepatology, Hôpital Cochin, Assistance Publique-Hôpitaux de Paris, 75014 Paris, France

[e] Department of Radiology, Hôpital Robert Debré, CRESTIC, URCA, 51000 Reims, France

[f] Department of Pathology, Hôpital Cochin, AP-HP, 75014 Paris, France

Corresponding author: maxime.barat@aphp.fr

Department of Radiology, Hôpital Cochin, AP-HP, 27 Rue du Faubourg Saint-Jacques, 75014 Paris, France

LI-RADS v2018 major criteria: do hepatocellular carcinomas in non-alcoholic steatohepatitis differ from those in virus-induced chronic liver disease on MRI?

Abstract

Purpose: LI-RADS v2018 diagnostic system is used to diagnose hepatocellular carcinoma (HCC) in at risk patients. However, its applicability to HCC in non-alcoholic steatohepatitis (NASH) has not been specifically studied. The purpose of this study was to assess the applicability of LI-RADS v2018 diagnostic system for HCC in patients with NASH.

Materials and methods: The MRI examinations of 41 patients with HCC and NASH (NASH group) were reviewed and compared to those obtained in 41 patients with HCC and virus-induced chronic liver disease (Virus group)**.** MRI examinations of the two groups were compared for imaging presentation, LI-RADS major criteria and LI-RADS categorization. Qualitative variables were compared using Fisher exact test and quantitative variables using Mann-Whitney U-test. Interreader agreement was assessed using kappa statistic.

Results: No significant differences in qualitative and quantitative variables were observed between the two groups. Most common findings in the two groups were hyperenhancement during the arterial phase and visibility on T2-weighted images (93% vs. 98%, $P = 0.616$ and 85% vs. 88%, $P = 1.000$ for NASH group and Virus group, respectively). No differences in prevalence between the two groups were found for any major LI-RADS v2018 criterion. Interreader agreement for LI-RADS categorization was strong for the NASH group (kappa = 0.802) and moderate for the virus group (kappa = 0.720). No differences were found between the two groups for LI-RADS categories ($P = 0.303$).

Conclusions: The LI-RADS v2018 diagnostic algorithm can be applied in patients with NASH.

Keywords: Carcinoma, Hepatocellular (Unique ID, D006528); Magnetic Resonance Imaging (Unique ID, D008279); Non-Alcoholic Fatty Liver Disease (Unique ID, D065626); Liver neoplasms (Unique ID, D008113);

Abbreviations

CT: computed tomography

DWI: diffusion-weighted imaging

HBV: hepatitis B virus

HCC: hepatocellular carcinoma

HCV: hepatitis C virus

LI-RADS: Liver Imaging Reporting and Data System

MRI: magnetic resonance imaging

NAFLD: non-alcoholic fatty liver disease

NASH: non-alcoholic steatohepatitis

1. INTRODUCTION

The majority of hepatocellular carcinomas (HCCs) develop in patients with liver cirrhosis [1]. Although chronic hepatitis B virus (HBV) and hepatitis C virus (HCV) related liver cirrhosis are the first causes of HCC worldwide, alcohol-related liver disease and non-alcoholic fatty liver disease (NAFLD) are now the main causes of liver cirrhosis and HCC in western countries [1]. NAFLD is a large spectrum of different or intricate conditions that include hepatic steatosis, non-alcoholic steatohepatitis (NASH), fibrosis, cirrhosis and end stage liver disease [2]. NASH is defined by necro-inflammatory reactions, hepatocyte ballooning and hepatocellular steatosis, resulting in a progressive disease leading to hepatic fibrosis and cirrhosis [2, 3]. Several reports showed that HCC can develop in the setting of NASH, with a continuously rising incidence [3, 4]. It is estimated that 4-27 % of patients with advanced NASH (*i.e.*, NASH with cirrhosis) develop HCC [4]. The annual incidence of HCC in non-cirrhotic and cirrhotic stage of NASH is 0.03% and 1.35%, respectively [5].

The surveillance for HCC in patients with NASH has not yet been fully defined [3]. European and American guidelines recommend surveillance for HCC with ultrasonography on a six-month basis in patients with underlying advanced fibrosis or cirrhosis [6, 7]. However, patients with NASH are often overweight or obese making surveillance with ultrasonography difficult [8]. As a consequence, magnetic resonance imaging (MRI) can be used in patients with NASH to exclude or characterize a liver nodule [9].

The Liver Imaging Reporting and Data System (LI-RADS) has been developed to standardize computed tomography (CT) and MRI techniques, interpretation, reporting, diagnostic management recommendations, and data collection in patients at risk for HCC [10]. This diagnostic algorithm is based on the presence of several criteria and helps make a noninvasive diagnosis of HCC [11, 12, 13, 14]. However, these imaging criteria have been developed for HCCs occurring in patients with liver cirrhosis, and not specifically for those with HCCs arising in NASH [15]. In this regard, studies reporting MRI presentation of HCC in patients with NAFLD or NASH found that some features used for the LI-RADS categorization may be less frequently present by comparison

with HCC in patients with liver cirrhosis [9, 16, 17, 18], thus questioning the applicability of LI-RADS criteria for HCC in NASH. In addition, to date no studies have compared the MRI presentation of HCC in NASH to those arising in virus-induced chronic liver disease.

The purpose of this study was to determine whether the imaging presentation of HCCs in NASH differs from that of HCCs in virus-induced chronic liver disease on MRI and assess the applicability of LI-RADS diagnostic system for HCC in patients with NASH.

2. MATERIALS AND METHODS

2.1. Patients selection

This study received local ethics and institutional review board committee approval (AAA-2020-08029). The institutional review board waived the requirement for informed consent.

A retrospective search of the database of two institutions was performed to identify all patients with HCC and NASH who had MRI examination of the liver in the departments of radiology of the two institutions between January 2010 and October 2019. This initial search retrieved a total of 71 patients. MRI examinations and clinical files of these patients were analyzed to identify those with a full MRI protocol and definite histopathological confirmation of NASH and HCC. Inclusion criteria were: (*i*), histopathologically proven HCC and NASH; (*ii*), MRI examination of the liver available for review; and (*iii*), MRI performed before any treatment (in treatment-naïve patients). A total of 30 patients were excluded due to no definite histopathological confirmation of NASH (21 patients), incomplete MRI protocol (4 patients), or MRI examination obtained after percutaneous thermal ablation (5 patients). A total of 41 patients (32 from Institution 1 and 9 from Institution 2) with a definite diagnosis of HCC and NASH (NASH group) who had undergone MRI examination of the liver were included.

Forty-one patients (31 from Institution 1 and 10 from Institution 2) with HCC in virus-induced chronic liver disease (Virus group) were identified for matched comparison by the study coordinator (M.B.). They were extracted from a database of 324 patients with histopathologically confirmed HCC. These 41 patients were selected according to sex, and age, and had MRI examination during the same period with the same MRI protocols than those with HCC in NASH. In addition, the study coordinator selected the patients to obtain HCCs with similar dimensions and underlying parenchymal disease severity in the two groups. For the 41 patients, the diagnosis of HCC was obtained histopathologically before any treatment. The study flowchart is presented in Figure 1.

For all patients, clinical data (sex, age, underlying hepatic disease, treatment of HCC) and histopathological data from the HCC and the hepatic parenchyma were collected by the study coordinator.

2.2 Diagnosis of HCC and chronic liver disease

In the NASH group, the diagnosis of HCC was based on the results of histopathological analysis of biopsy specimens obtained from percutaneous biopsy in 39 patients (39/41; 95%) or after surgical resection in two patients (2/41; 5%). Tissue samples were also obtained from the liver parenchyma to document the status of the underlying hepatic disease as fibrosis or cirrhosis using percutaneous biopsy in all patients [19, 20]. In all patients, the diagnosis of NASH was originally established by a pathologist using the NASH Clinical Research Network criterion, 3- to 10-years before the occurrence of HCC [21]. NASH was also defined by the exclusion of HCV and HBV infection, alcohol abuse, primary biliary cirrhosis, primary sclerosing cholangitis, autoimmune hepatitis, hemochromatosis or Wilson disease.

In the Virus group, the diagnosis of HCC was based on the results of histopathological analysis of biopsy specimens obtained from percutaneous biopsy in 30 patients (30/41; 73%) or after surgical resection in 11 patients (11/41; 27%). Similar to NASH group, tissue samples were also obtained from the liver parenchyma to document the status of the underlying hepatic disease using percutaneous biopsy in all patients. Underlying fibrosis and cirrhosis were classified by a pathologist (B.T.) with 30 years of experience in liver diseases as F3 and F4, using the METAVIR score [22]. Viral infection was due to HBV (12/41; 29%), HCV (28/41; 68%) or HBV-HCV (1/41; 2%).

2.3. MRI protocol

The MR imaging protocol is detailed in **Table 1**. All patients underwent abdominal MRI examination using a 1.5-T system (Magnetom Avanto ® or Aera®, Siemens Healthineers, Erlangen, Germany). All patients had free breathing fat-suppressed T2-weighted turbo spin-echo (TSE), fat-suppressed breath-hold T2-weighted half-Fourier acquisition single-shot turbo spin-echo (HASTE), unenhanced in-phase and out-of- phase T1-weighted imaging, diffusion-weighted imaging (DWI) and fat-suppressed three-dimensional volumetric interpolated breath-hold gradient-echo (3D VIBE) sequences before and after intravenous administration of a gadolinium chelate. Examinations were performed with multichannel anterior and posterior phased-array coils.

In-phase and out-of-phase breath-hold T1-weighted sequences were acquired with a dual echo technique to obtain perfect registration between corresponding images [23]. Breath-hold fat-suppressed T1-weighted 3D VIBE sequences were performed in the transverse plane before and after intravenous administration of a gadolinium-based contrast agent (gadoterate meglumine, Dotarem®, Guerbet, Roissy-Charles de Gaulle, France) at a dose of 0.1-mmol/kg of body weight and an injection rate of 2.5 mL/sec in 32 patients of NASH group and 33 patients of Virus group) or gadobenate dimeglumine (Gd-BOPTA, Multihance®, Bracco Imaging, Milan, Italy) at a dose of 0.03-mmol/kg of body weight and an injection rate of 2.5 mL/sec in 9 patients of NASH group and 8 patients of Virus group) followed by a 20-mL saline flush, using a power injector (Optistar®, Guerbet or Spectris® Solaris EP, Medrad, Pittsburg, PA, USA) at an injection rate of 2-2.5 mL/sec. Four acquisitions were obtained after administration of contrast material, at 25 sec, 70 sec, 180 sec, and 5 min. All 3D VIBE acquisitions were performed during breath hold at end expiration.

2.4. MR image analysis

MRI examinations were analyzed on a picture archiving and communication system (PACS) viewing station (Directview, 12.1.1.1059 version, Carestream Health Inc, Rochester, NY, USA) using a standardized data collection form. To minimize review bias, the radiologists were blinded to any patient information. All MRI sequences were assessed as a single set for each individual patient. In patients with more than one HCC nodule, a single nodule for which histopathological confirmation was obtained was analyzed. A first reading session was made by two radiologists who performed quantitative and qualitative analyses of all MRI examinations in consensus, blinded to the nature of the underlying hepatic disease. Then, one radiologist and one hepatologist analyzed independently MRI examinations for the presence of LI-RADS v2018 major criteria and LI-RADS v2018 classification [24, 25], blinded to the original interpretation of the first reading session.

2.4.1. Qualitative analysis

Several qualitative variables were evaluated by the same two radiologists working in consensus. They included tumor location (right *vs.* left liver), tumor hyper enhancement during the arterial phase, tumor wash out during the portal or delayed phase, corona sign (zone or rim of peri-observation enhancement in the late arterial phase or early portal venous phase occurring after rapid dissipation of contrast material from an arterial phase hyperenhancing mass), tumor fat content (tumor signal drop between in- and out-of-phase T1-weighted images), tumor visibility on

unenhanced T1-weighted images, tumor visibility on T2-weighted images, tumor capsule (smooth, uniform, sharp border or rim around most or all of the observation), portal vein invasion by HCC, and involvement of adjacent organs by HCC. All variables were defined according well-established criteria [13, 14, 25, 27, 28, 29, 30, 31].

2.4.2. Quantitative analysis

HCC nodules were analyzed by two radiologists (T.L.N., P.S.) working in consensus with respect to tumor length (*i.e.*, largest axial diameter from outer edge to outer edge), tumor signal drop (in %) between in-phase and out-of-phase T1-weighted MR images, and apparent diffusion coefficient (ADC) values. Tumor dimensions were measured using calipers in the axial plane by the two radiologists on magnified images obtained during the arterial dominant phase [26]. ADC measurements of HCC were made using semi-automatic regions of interest (ROI) drawn on DWI obtained with the lowest b value and then transferred on to the ADC map. The ADC maps were generated automatically from the source data using the integrated Syngo® software (Siemens Healthineers). ADC values were calculated using a mono-exponential fitting algorithm. ADC values were obtained from the whole HCC with a 1-mm peripheral margin of lesion left outside the ROI to avoid including adjacent hepatic parenchyma within the ROI. ADC values were obtained three times and the three measurements were averaged.

2.4.3. LI-RADS assessment

LI-RADS categorization was performed by one radiologist (J.-B. C.) and one hepatologist (Cl.H.) working independently. Each target HCC was assessed by both readers for lesion size (≥ 20 mm) on arterial phase image, non-rim arterial phase hyperenhancement, presence of non-peripheral washout and peripheral capsule. HCCs were further assigned a LI-RADS category following LI-RADS v2018 major criteria [24, 25]. Threshold growth was not considered. The two observers were blinded to the results of previous quantitative and qualitative analyses and to the nature of the underlying parenchymal disease but knew that all lesions were HCCs. At the end of the independent readings, discordant readings were resolved by consensus.

2. 5. Statistical analysis

Statistical analysis was performed using SAS software (version 9.2, SAS Institute, Cary, NC; RV.3 4-0R Foundation, http://www.r-project.org/). Descriptive statistics were calculated for all variables

evaluated at MRI. Quantitative (continuous) variables were reported as means ± standard deviations (SD), medians, first (Q1) and third (Q3) quartiles and ranges. Qualitative (binary) variables were reported as raw numbers, proportions, and percentages.

Comparisons of quantitative variables between the two groups were performed using Mann-Whitney U test. Comparisons of qualitative variables and LI-RADS v2018 major criteria were made using Fisher exact test. Significance was set at $P < 0.05$. Agreement between observers for LI-RADS categorization was assessed with kappa-test. Kappa values were reported with their 95% confidence intervals (CI) [32]. Kappa values of 0.00-0.20; 0.21-0.40; 0.41-0.60; 0.61-0.80; and 0.81-1.00 were considered to indicate slight, fair, moderate, substantial, and almost perfect agreement, respectively.

3. RESULTS

3.1. Study population

The NASH group included 34 men and 7 women with a mean age of 67.9 ± 10.6 (SD) years and the Virus group included 34 men and 7 women, with a mean age of 64.6 ± 12.9 (SD) years. Demographic characteristics of the study population are reported in **Table 2**. No differences in age ($P = 0.233$) and sex distribution ($P = 1.000$) were found between the two groups. No differences in underlying liver parenchyma disease were found between the NASH group (S3, 9/41 patients, 22%; S4, 32/41 patients, 78%) and the Virus group (F3, 11/41 patients, 27%; F4, 30/41 patients, 73%) ($P = 0.801$).

3.2. Univariate analysis

Distribution of quantitative and qualitative variables in the two groups as observed during the consensus reading are reported in **Table 3**. Hyperenhancement during the arterial phase was the most common finding in the two groups (93% [38/41] in the NASH group and 98% [40/41] in the virus group; $P = 0.616$), followed by visibility on T2-weighted images (85% [35/41] in the NASH group and 88% [36/41] in the Virus group; $P = 1.000$). No significant differences in quantitative and qualitative variables were observed between the two groups. However, a tendency toward less

frequent portal washout was observed in the NASH group although not significant (P = 0.080) and not affecting LI-RADS categorization.

3.3. LI-RADS categorization

The results of independent reading for the presence of major LI-RADS v2018 criteria are reported in **Table 4**. For both readers, tumor hyperenhancement during the arterial phase was the most commonly observed LI-RADS v2018 criterion, with kappa values of 0.626 in the NASH group and 0.655 in the Virus group (**Figures 2, 3**). Tumor capsule in NASH group was the criterion with the lowest kappa value (kappa = 0.367; weak agreement) (**Figures 3, 4**).

No differences in prevalence of major LI-RADS v2018 criteria between NASH and Virus groups were found for both readers, including wash out feature (P = 0.800 and 0.198) (**Figure 5, Table 4**). Inter reader agreement for LI-RADS categorization was strong for the NASH group (kappa = 0.802) and moderate for the Virus group (kappa = 0.720) (**Table 4**).

Results of consensus reading for LI-RADS categorization are reported in **Table 3**. No differences in LI-RADS categories were found between the two groups (P = 0.303).

4. DISCUSSION

In our study that included 41 patients with HCC and NASH and 41 patients with HCC and virus-induced chronic liver disease matched for age, sex, severity of underlying hepatic disease and tumor size, we found that HCC in NASH mostly manifests as a hyperenhancing tumor (88%-90%) during the arterial phase after intravenous administration of a gadolinium-based contrast agent, with tumor capsule (61%-76%), wash out (63%-68%) and a diameter ≥ 20 mm (61%). Most importantly, no differences in MRI presentation were found between HCC in NASH and HCC in virus-induced chronic liver disease, resulting in similar LI-RADS categorization by two independent readers and supporting the application of LI-RADS v2018 major criteria for HCC in NASH.

Alsharan et al. have reported the MRI features of 30 HCC nodules in 21 patients with NASH [9]. They reported that 40% (12/30) of HCC nodules did not display the “wash-out” feature during the portal or delayed phase of enhancement [9]. They have suggested that imaging criteria that have been developed for the non-invasive diagnosis of HCC should be applied with caution to HCC in patients with NASH [9]. However, they did not assess to what extent this feature may alter LI-RADS categorization. In the present study, we found that the difference in prevalence of the “wash-out” feature did not differ between HCC in NASH and HCC in virus-induced chronic liver

disease. On the opposite, in the study by Thompson et al. that included 48 patients with NAFLD, HCC showed no wash-out in only 21% of patients (10/48) on MRI compared to 32%-37% in patients with NASH in our study [17]. These researchers suggested that the absence of wash-out correlated with increasing hepatic steatosis [17]. In our study, all patients had NASH with underlying hepatic fibrosis (S3) or cirrhosis (S4) with limited of absent steatosis (*i.e.*, "burn-out" NASH), thus possibly explaining differences in prevalence of wash-out feature. However, using CT, Kim et al. found that the presence of underlying hepatic steatosis did not affect the prevalence of the wash-out feature, suggesting that this phenomenon may be more complex than related to attenuation differences only [33].

In LI-RADS, hyperenhancement during the arterial phase refers to the presence of non-rimlike enhancement in all or portion of a nodule that is greater than that of the surrounding hepatic parenchyma [33]. This finding is a major criterion in LI-RADS v2018 and is more sensitive than the other dynamic criteria for the diagnosis of HCC on MRI [13, 34, 35]. In the present study, non-rimlike hyperenhancement during the arterial phase after intravenous administration of a gadolinium-based contrast agent was observed in 37/41 (90%) and 36/41 (88%) HCCs in NASH by two independent readers. These results are in line with those of Alsharan et al., who reported non-rimlike hyperenhancement during the arterial phase in 30/30 HCCs (100%) in patients with NASH [9]. Similar results were obtained by Thompson et al. in 48 patients with HCC in NAFLD, in whom arterial phase hyperenhancement was present in 45/48 patients (93%) [17].

Tumor capsule is defined as the presence of a smooth, uniform, sharp border around a liver nodule, in total or incompletely, presenting as enhancing rim on portal or later phase images [34, 36]. When used alone on MRI, capsule appearance has sensitivities and specificities for the diagnosis of HCC that vary according to nodule size [37]. In our study, capsule was observed in 52/82 HCCs (63%) in the whole study population with no differences between NASH and virus groups. Those results are in line with those of Alsharan et al. who reported tumor capsule in 60% (18/30) HCCs in NASH [9]. Similarly, Iannacconne et al. and Thompson et al. reported tumor capsule in 68 % (15/22) and 71% (34/48) HCC in NAFLD, respectively [16, 17]. When used alone as a major criterion, tumor capsule had 32.9% sensitivity and 98.8% specificity for the diagnosis of HCC in the study by Cerny et al. [38]. However, these researchers did not indicate the nature of the underlying liver disease of their patients [38].

Our study has some limitations. First, our objective was to compare HCC in NASH to HCC in virus-induced chronic liver disease using LI-RADS v2018 major criteria so that ancillary criteria were not analyzed. Second, all patients had HCC so that we did not assess the capabilities of MRI in discriminating between HCC and other hepatic tumors [39]. Third, a subset of patients received

gadobenate dimeglumine, which a hepatocyte selective contrast agent [35]. However, the hepatobiliary phase was not included in the image analysis and the distribution of contrast materials was well balanced between NASH and Virus groups, thus limiting potential bias. Fourth, our comparison was restricted to HCC for which histopathological confirmation was obtained, thus introducing inclusion bias as only one HCC in an individual patient was used for comparison. Fifth, the design of the study did not allow to evaluate LI-RADS classes 1, 2 and 3 because only histopathologically proven HCC were included. Sixth, the mean size of HCC was quite large (30 mm in NASH group and 38 mm in Viral group) so that small HCC with atypical features might have been excluded. Sixth we did not evaluate LI-RADS ancillary features, but they have utility to increase sensitivity but not specificity for the diagnosis of HCC [38]. Finally, considering that most of our patients had S4 or F4 underlying chronic liver disease, this may be a limitation to extrapolate our results to a more general population.

In conclusion, we have described the MRI features of HCC in NASH in 41 patients. HCC in NASH shows MRI features similar to those of HCC in virus-induced chronic liver disease resulting in similar LI-RADS categorization by two independent readers. Our results suggest the applicability of LI-RADS v2018 major criteria for HCC in NASH.

Authorship requirements: All the authors had fully participated to the study and approved the final draft.

Conflicts of interest. The authors have no conflicts of interest to disclose in relation with this study.

Funding. This research received no financial support**.**

References

1. Yang JD, Hainaut P, Gores GJ, Amadou A, Plymoth A, Roberts LR. A global view of hepatocellular carcinoma: trends, risk, prevention and management. Nat Rev Gastroenterol Hepatol 2019;16: 589–604.

2. Diehl AM, Day C. Cause, pathogenesis, and treatment of nonalcoholic steatohepatitis. N Engl J Med 2017;377: 2063–2072.

3. Massoud O, Charlton M. Nonalcoholic fatty liver disease/nonalcoholic steatohepatitis and hepatocellular carcinoma. Clin Liver Dis 2018;22: 201–211.

4. Ascha MS, Hanouneh IA, Lopez R, Tamimi TA, Feldstein AF, Zein NN. The incidence and risk factors of hepatocellular carcinoma in patients with nonalcoholic steatohepatitis. Hepatology 2010;51: 1972–1978.

5. Tarao K, Nozaki A, Ikeda T, Sato A, Komatsu H, Komatsu T, et al. Real impact of liver cirrhosis on the development of hepatocellular carcinoma in various liver diseases-meta-analytic assessment. Cancer Med 2019;8: 1054-1065.

6. Kolly P, Dufour JF. Surveillance for hepatocellular carcinoma in patients with NASH. Diagnostics 2016;6: E22.

7. EASL Clinical Practice Guidelines: Management of hepatocellular carcinoma. J Hepatol 2018;69: 182–236.

8. Yasui K, Hashimoto E, Komorizono Y, Koike K, Arii S, Imai Y et al. Characteristics of patients with nonalcoholic steatohepatitis who develop hepatocellular carcinoma. Clin Gastroenterol Hepatol 2011;9: 428–433.

9. Al-Sharhan F, Dohan A, Barat M, Feddal A, Terris B, Pol S, Mallet V, Soyer P. MRI presentation of hepatocellular carcinoma in non-alcoholic steatohepatitis (NASH). Eur J Radiol 2019;119: 108648.

10. Shah A, Tang A, Santillan C, Sirlin C. Cirrhotic liver: what's that nodule? The LI-RADS approach. J Magn Reson Imaging 2016;43: 281–294.

11. Ronot M, Purcell Y, Vilgrain V. Hepatocellular carcinoma: current imaging modalities for diagnosis and prognosis. Dig Dis Sci 2019; 64: 934–950.

12. McEvoy SH, McCarthy CJ, Lavelle LP, Moran DE, Cantwell CP, Skehan SJ et al. Hepatocellular carcinoma: illustrated guide to systematic radiologic diagnosis and staging according to guidelines of the American Association for the Study of Liver Diseases. Radiographics 2013;33: 1653–1668.

13. Rimola J, Forner A, Tremosini S, Reig M, Vilana R, Bianchi L, et al. Non-invasive diagnosis of hepatocellular carcinoma ≤ 2 cm in cirrhosis: diagnostic accuracy assessing fat, capsule and signal intensity at dynamic MRI. J Hepatol 2012;56: 1317–1323.

14. Ronot M, Fouque O, Esvan M, Lebigot J, Aubé C, Vilgrain V. Comparison of the accuracy of AASLD and LI-RADS criteria for the non-invasive diagnosis of HCC smaller than 3 cm. J Hepatol 2018;68: 715–723.

15. Di Martino M, Saba L, Bosco S, Rossi M, Miles KA, Di Miscio R et al. Hepatocellular carcinoma (HCC) in non-cirrhotic liver: clinical, radiological and pathological findings. Eur Radiol 2014;24: 1446–1454.

16. Iannaccone R, Piacentini F, Murakami T, Paradis V, Belghiti J, Hori M et al. Hepatocellular carcinoma in patients with nonalcoholic fatty liver disease: helical CT and MR imaging findings with clinical-pathologic comparison. Radiology 2007;243: 422–430.

17. Thompson SM, Garg I, Ehman EC, Sheedy SP, Bookwalter CA, Carter RE et al. Non-alcoholic fatty liver disease-associated hepatocellular carcinoma: effect of hepatic steatosis on major hepatocellular carcinoma features at MRI. Br J Radiol 2018;91: 20180345.

18. Mamone G, Di Piazza A, Carollo V, Crinò F, Vella S, Cortis K, Miraglia R. Imaging of primary malignant tumors in non-cirrhotic liver. Diagn Interv Imaging 2020;101: 519–535.

19. Brunt EM, Janney CG, Di Bisceglie AM, Neuschwander-Tetri BA, Bacon BR. Nonalcoholic steatohepatitis: a proposal for grading and staging the histological lesions. Am J Gastroenterol 1999; 94: 2467–2474.

20. Takahashi Y, Fukusato T. Histopathology of nonalcoholic fatty liver disease/nonalcoholic steatohepatitis. World J Gastroenterol 2014;20: 15539-15548.

21. Kleiner DE, Brunt EM, Van Natta M, Behling C, Contos MJ, Cummings OW et al. Design and validation of a histological scoring system for nonalcoholic fatty liver disease. Hepatology 2005; 41: 1313–1321.

22. The French METAVIR Cooperative Study Group. Intraobserver and interobserver variations in liver biopsy interpretation in patients with chronic hepatitis C. Hepatology 1994;20: 15-20.

23. Merkle EM, Nelson RC. Dual gradient-echo in-phase and opposed-phase hepatic MR imaging: a useful tool for evaluating more than fatty infiltration or fatty sparing. Radiographics 2006;26: 1409–1418.

24. American College of Radiology. CT/MRI LI-RADS v2018 core. Liver Imaging Reporting and Data System. https://nrdr.acr.org/lirads/. 2018.

25. Elsayes KM, Kielar AZ, Elmohr MM, Chernyak V, Masch WR, Furlan A, et al. White paper of the Society of Abdominal Radiology hepatocellular carcinoma diagnosis disease-focused panel on LI-RADS v2018 for CT and MRI. Abdom Radiol 2018;43: 2625–2642.

26. Cunha GM, Kwon H, Wolfson T, Gamst AC, Chung YE, Kim MJ, et al. Examining LI-RADS recommendations: should observation size only be measured on non-arterial phases? Abdom Radiol 2020;doi: 10.1007/s00261-020-02490-x.

27. Sandrasegaran K, Tahir B, Nutakki K, Akisik FM, Bodanapally U, Tann M, et al. Usefulness of conventional MRI sequences and diffusion-weighted imaging in differentiating malignant from benign portal vein thrombus in cirrhotic patients. AJR Am J Roentgenol 2013;201: 1211–1219.

28. Ehman EC, Behr SC, Umetsu SE, Fidelman N, Yeh BM, Ferrell LD, et al. Rate of observation and inter-observer agreement for LI-RADS major features at CT and MRI in 184 pathology proven hepatocellular carcinomas. Abdom Radiol 2016; 41: 963–969.

29. Unal E, Idilman IS, Akata D, Ozmen MN, Karcaaltincaba M. Microvascular invasion in hepatocellular carcinoma. Diagn Interv Radiol 2016;22: 125–132.

30. Jamwal R, Krishnan V, Kushwaha DS, Khurana R. Hepatocellular carcinoma in non-cirrhotic versus cirrhotic liver: a clinico-radiological comparative analysis. Abdom Radiol 2020; doi: 10.1007/s00261-020-02561-z.

31. Chernyak V, Tang A, Flusberg M, Papadatos D, Bijan B, Kono Y, et al. LI-RADS® ancillary features on CT and MRI. Abdom Radiol 2018;43: 82–100.

32. Benchoufi M, Matzner-Lober E, Molinari N, Jannot AS, Soyer P. Interobserver agreement issues in radiology. Diagn Interv Imaging 2020;101: 639–641.

33. Kim SS, Hwang JA, Shin HC, Choi SY, Kang TW, Jou SS, et al. LI-RADS v2017 categorization of HCC using CT: does moderate to severe fatty liver affect accuracy. Eur Radiol 2019;29: 186–194.

34. Tang A, Bashir MR, Corwin MT, Cruite I, Dietrich CF, Do RKG, et al; LI-RADS Evidence Working Group. Evidence supporting LI-RADS major features for CT- and MR imaging-based diagnosis of hepatocellular carcinoma: a systematic review. Radiology 2018;286: 29–48.

35. Kim TK, Lee KH, Jang HJ, Haider MA, jacks LM, Menezes RJ, et al. Analysis of gadobenate dimeglumine-enhanced MR findings for characterizing small (1-2-cm) hepatic nodules in patients at high risk for hepatocellular carcinoma. Radiology 2011;259: 730–738.

36. Okuda K, Musha H, Nakajima Y, Kubo Y, Shimokawa Y, Nagasaki Y, et al. Clinicopathologic features of encapsulated hepatocellular carcinoma: a study of 26 cases. Cancer 1977;40: 1240–1245.

37. Khan AS, Hussain HK, Johnson TD, Weadock WJ, Pelletier SJ, Marrero JA. Value of delayed hypointensity and delayed enhancing rim in magnetic resonance imaging diagnosis of small hepatocellular carcinoma in the cirrhotic liver. J Magn Reson Imaging 2010;32: 360–366.

38. Cerny M, Bergeron C, Billiard JS, Murphy-Lavallée J, Olivié D, Bérubé J, et al. LI-RADS for MR imaging diagnosis of hepatocellular carcinoma: performance of major and ancillary features. Radiology 2018;288: 118-128.

39. Elsayes KM, Fowler KJ, Chernyak V, Elmohr MM, Kielar AZ, Hecht E, et al. User and system pitfalls in liver imaging with LI-RADS. J Magn Reson Imaging 2019;50: 1673–1686.

Figure legends

Figure 1. Study flowchart. MRI indicates magnetic resonance imaging. NASH indicates non-alcoholic steatohepatitis. HCC indicates hepatocellular carcinoma.

Figure 2. 68-year-old man with hepatocellular carcinoma at the hepatic dome (segment IV) and nonalcoholic steatohepatitis (S3 fibrosis).
A, T1-weighted MR image obtained during the arterial phase following intravenous administration of a gadolinium chelate in the axial plane shows hyperenhancing focal liver lesion at the hepatic dome (arrow).
B, T1-weighted MR image obtained during the portal phase reveals focal liver lesion displaying tumor capsule.
C, On T1-weighted MR image obtained 3 min following intravenous administration of a gadolinium chelate in the axial plane, the focal liver lesion displays wash out feature (arrow).

Figure 3. 83-year-old man with hepatocellular carcinoma in segment V and virus-induced chronic liver disease (F4 cirrhosis).
A, T1-weighted MR image obtained during the arterial phase following intravenous administration of a gadolinium chelate in the axial plane shows hyperenhancing focal liver lesion in the right liver (arrow).
B, T1-weighted MR image obtained during the portal phase reveals no wash-out of the lesion (arrow). Tumor capsule was considered present by one reader and absent by the other reader during independent reading sessions.

Figure 4. 62-year-old man with hepatocellular carcinoma in segment V and nonalcoholic steatohepatitis (S3 fibrosis). T1-weighted MR image obtained during the portal phase reveals wash-out. Capsule was considered present by one reader while the other reader considered mass effect by tumor on adjacent vessels during independent reading sessions.

Figure 5. 59-year-old man with hepatocellular carcinoma in segments VII-VIII and nonalcoholic steatohepatitis (S4 cirrhosis).

A, T1-weighted MR image obtained during the arterial phase following intravenous administration of a gadolinium chelate in the axial plane shows hyperenhancing focal liver lesion in the right liver (arrow).

B, T1-weighted MR image obtained during the portal phase reveals wash-out (arrow) and tumor capsule by two independent readers.

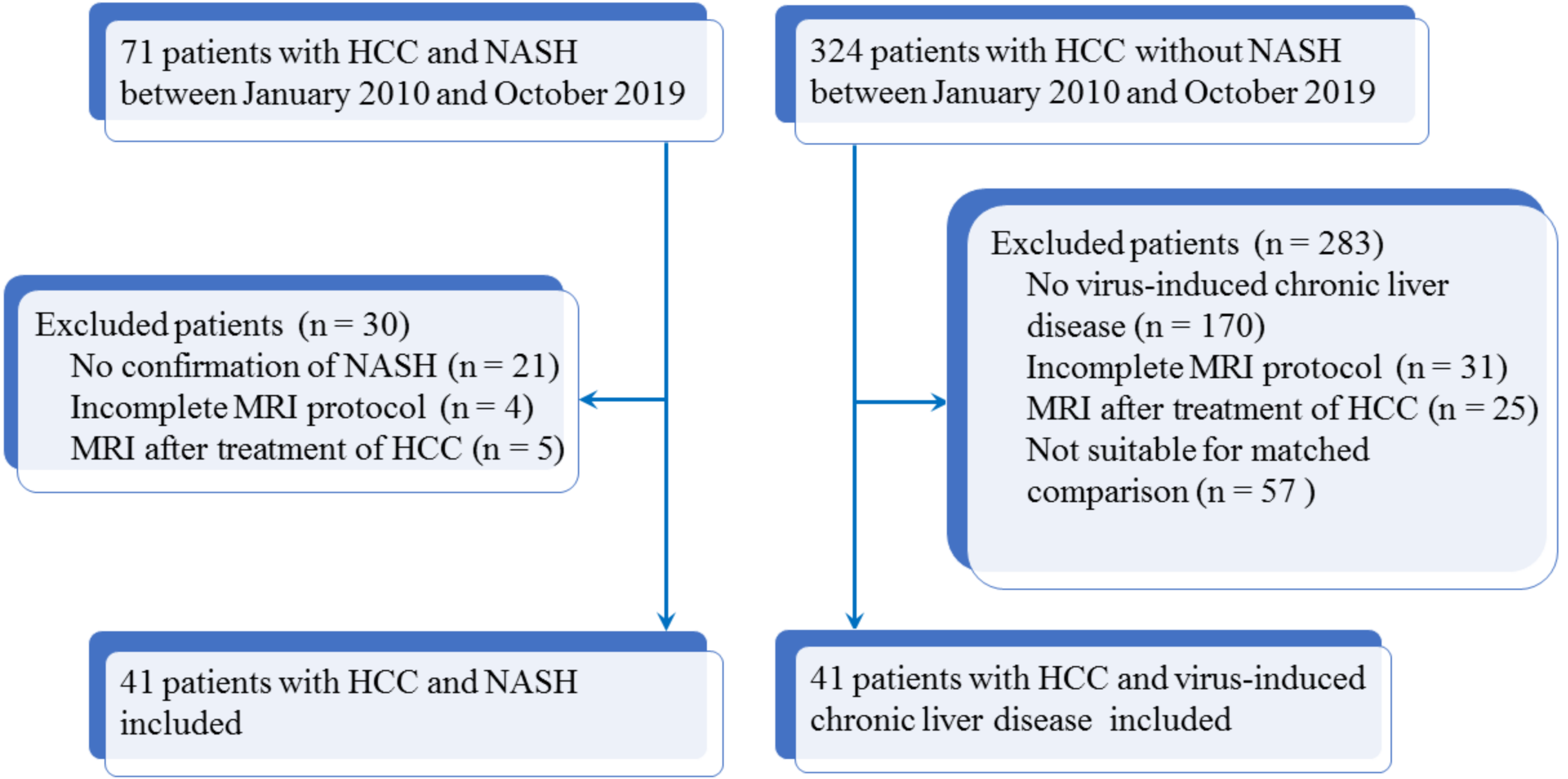
71 patients with HCC and NASH between January 2010 and October 2019
324 patients with HCC without NASH between January 2010 and October 2019
Excluded patients (n = 30)
No confirmation of NASH (n = 21)
Incomplete MRI protocol (n = 4)
MRI after treatment of HCC (n = 5)
Excluded patients (n = 283)
No virus-induced chronic liver disease (n = 170)
Incomplete MRI protocol (n = 31)
MRI after treatment of HCC (n = 25)
Not suitable for matched comparison (n = 57)
41 patients with HCC and NASH included
41 patients with HCC and virus-induced chronic liver disease included

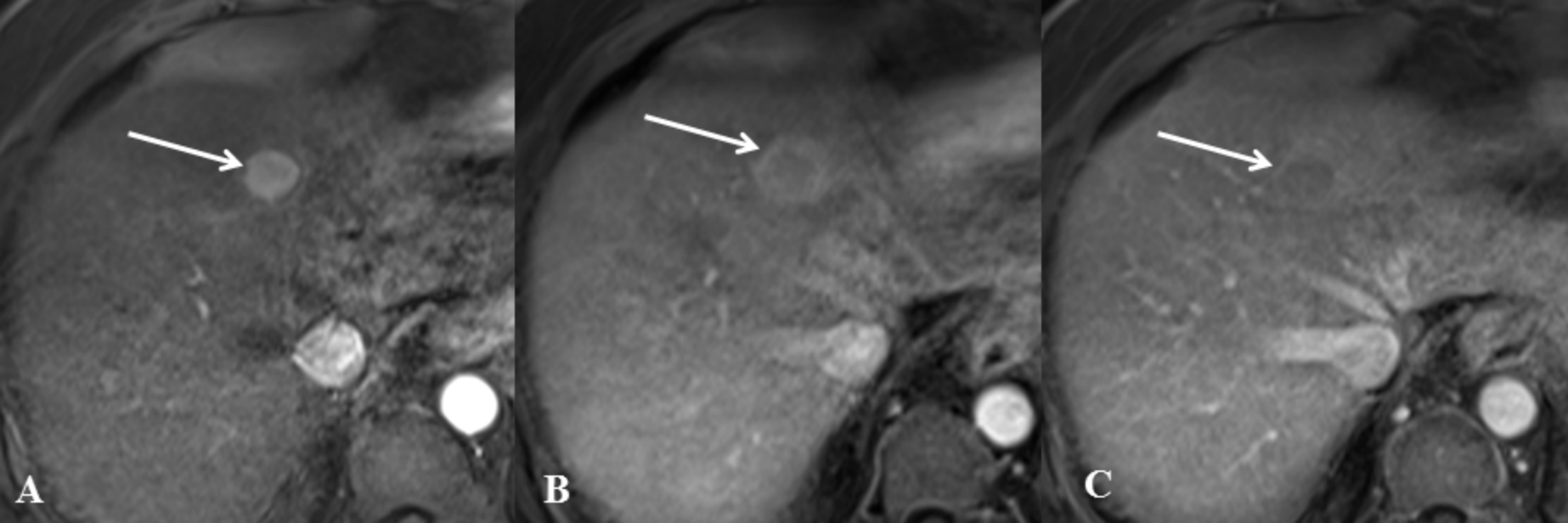
A
B
C

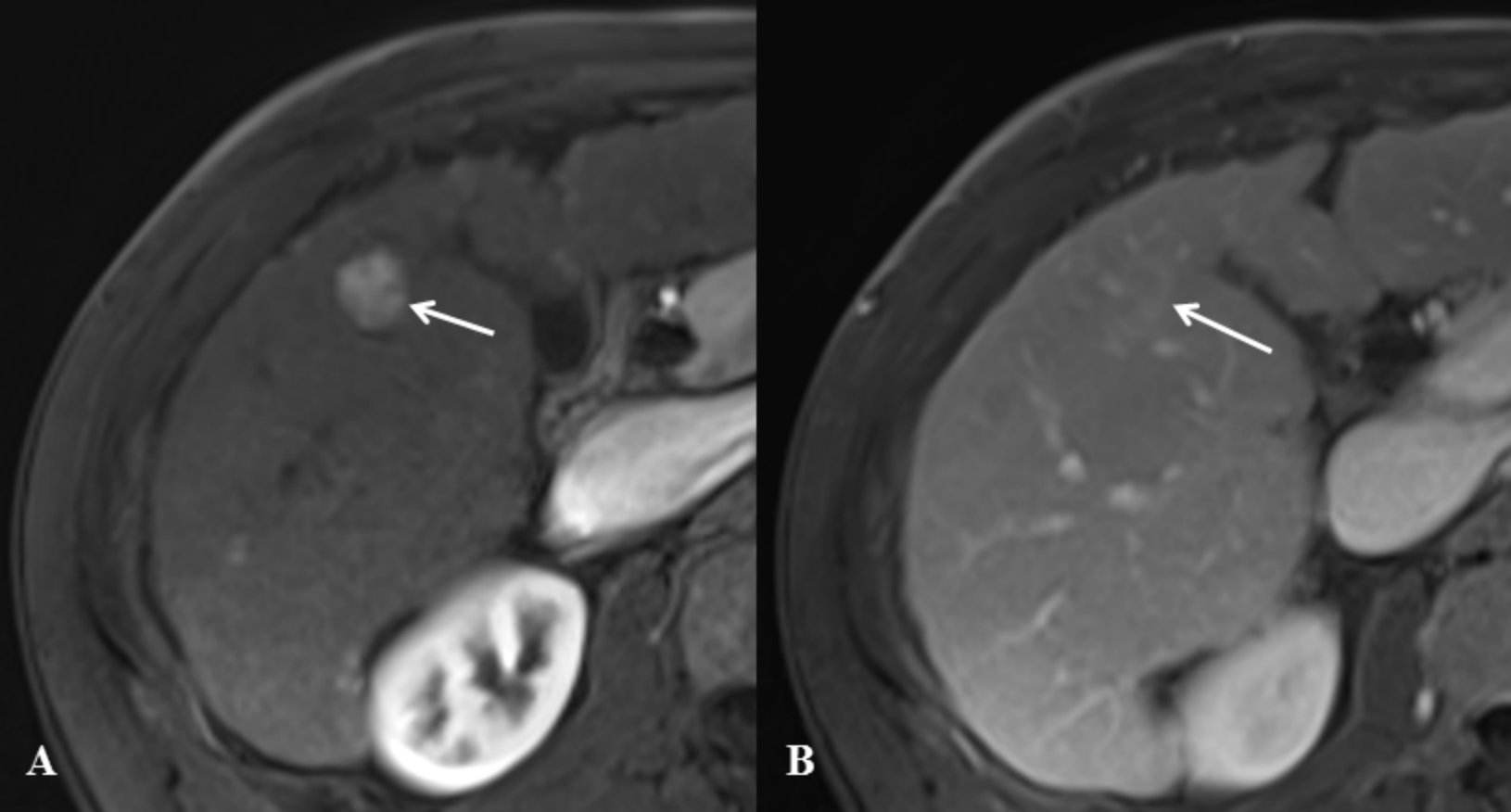
A
B

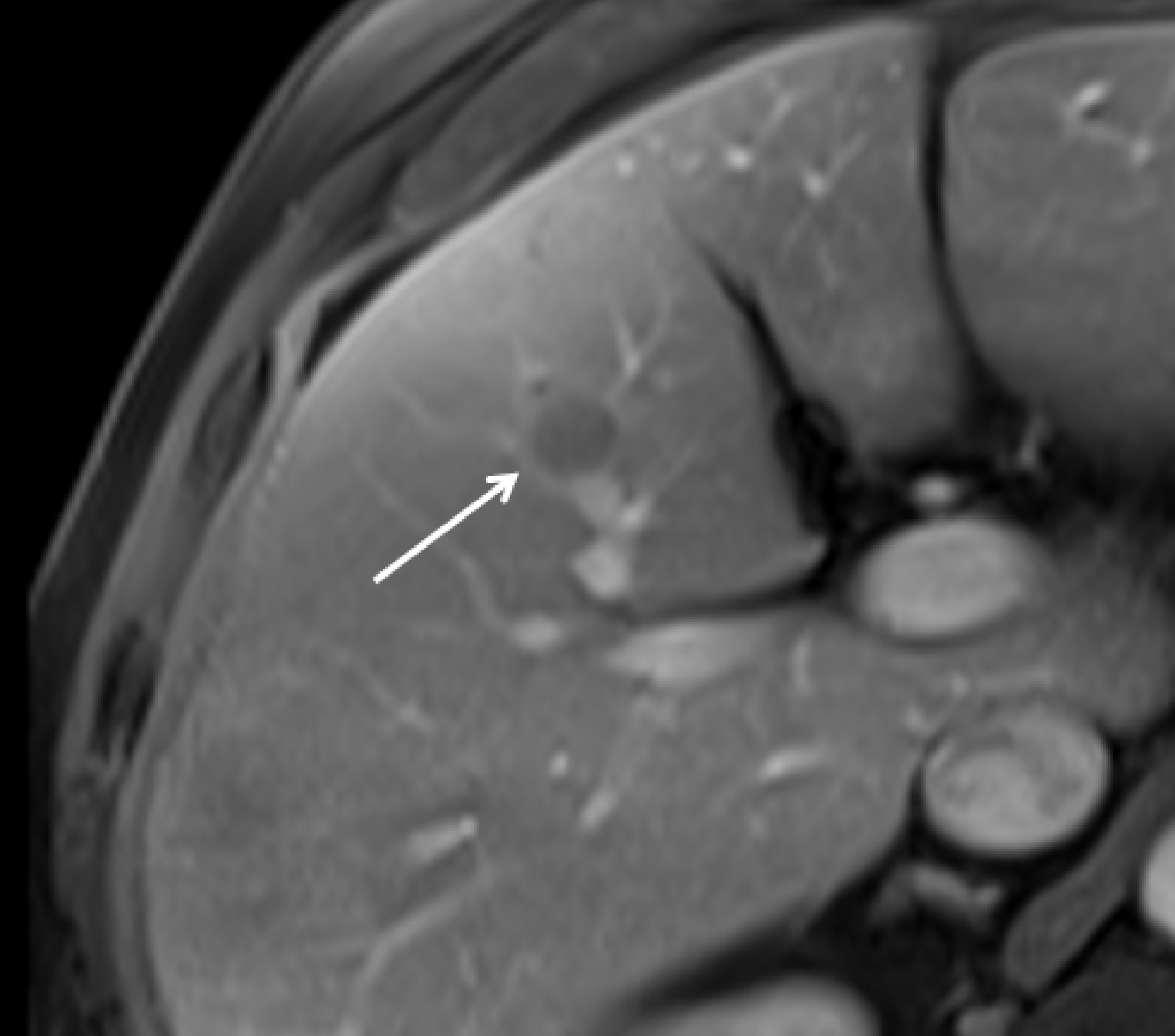

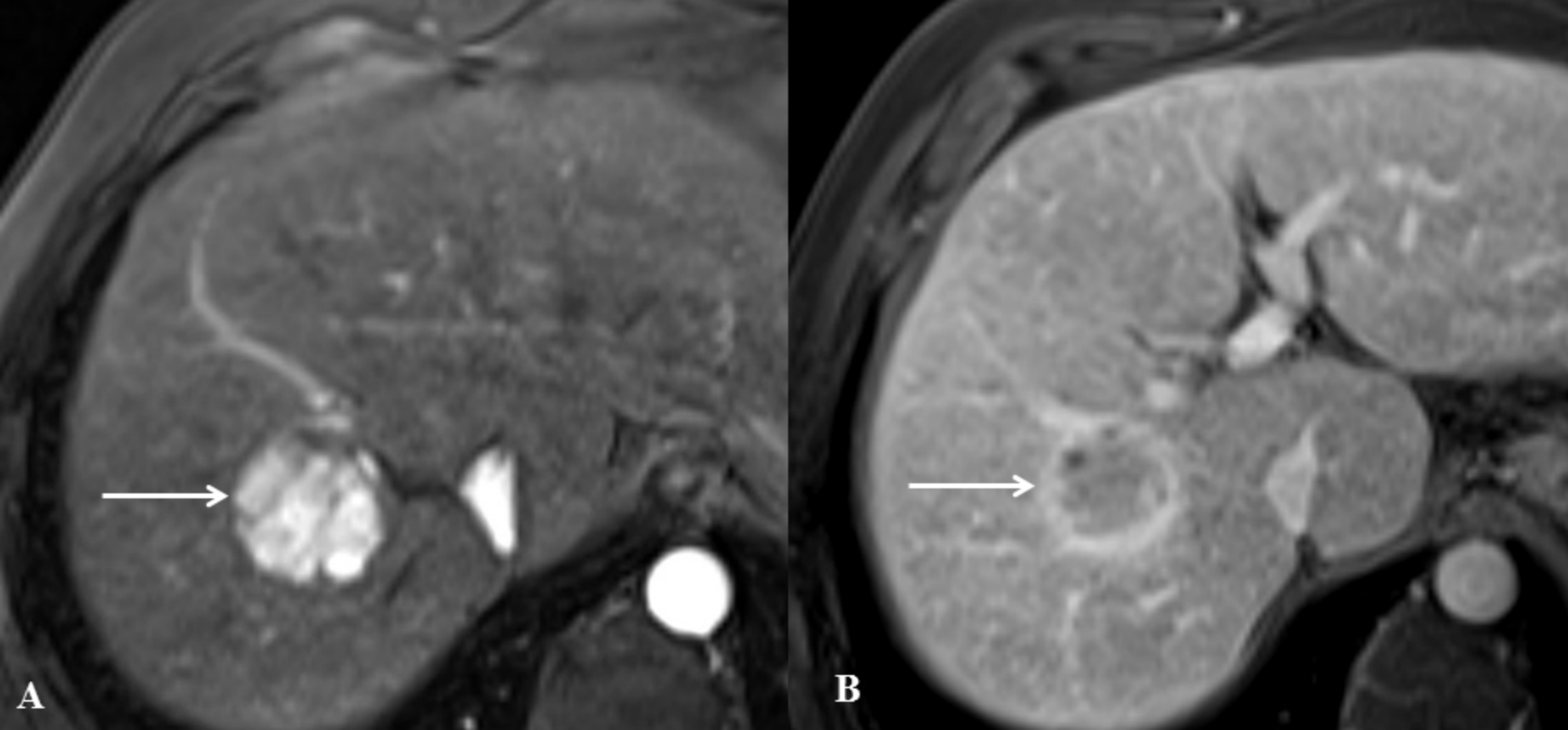
A
B

Table 1. MRI parameters

	T1 in phase	**T2 TSE**	**T2 HASTE**	**DWI**	**T1 3D VIBE**
Plane	Axial	Axial	Axial	Axial	3D (Axial)
Repetition time (ms)*	6.4-110	3750-7058	1000-1200	3900-5500	3.90-5.45
Echo time (ms)	2.56-4.77	88-121	89-95	67-91	1.48-2.03
Flip angle (°)[ǂ]	9-10	175-180	150	90	9, 10, 12, 14
Echo train length	1-2	14-17	75-256	40-57	1
Fat suppression	No	Yes	No	Yes	Yes
Slice thickness (mm)	3-7.5[†]	4-7	4.5-6	5-6	2.2-4
Intersection gap (mm)	0-1	0-1.6	0-1	1-2	0
Number of slices	24-80	24	19-24	25-30	64-120
Reconstruction matrix size	290-512 × 182-512	230-512 × 320-512	200-256 × 198-256	144-182 × 192	166-234 × 320-384
Field of view (mm)	320-340 × 320-340	320-340 × 320-340	320-340 × 320-340	252-340 × 320-400	320-340 × 320-340
Acquisition time (sec)	19-28	120-300	24-30	120-257	10-26
Breath-hold	Yes	Free-breathing	Yes	Free-breathing	Yes

Note. N.A. indicates not applicable; DWI indicates diffusion-weighted imaging; TSE indicates turbo spin-echo; HASTE indicates fat-suppressed breath-hold T2-weighted half-Fourier acquisition single-shot turbo spin-echo; 3D VIBE indicates three-dimensional volumetric interpolated breath-hold gradient-echo. * Repetition time depended on the duration of the breath cycle. [†]A slice thickness of 7.5 mm was used in two patients. DWI was obtained with 3 b values of 50, 400-600, 800-1000 sec/mm^2. [ǂ] Flip angles may vary according to several parameters defined by the manufacturer.

Table 2. Demographic variables of 41 patients with HCC on NASH and 41 patients with HCC on virus-induced chronic liver disease

Variables	Whole study population (n = 82)	NASH (n = 41)	Virus (n = 41)	*P* value
Sex				1.000
Male	68 (83%)	34 (83%)	34 (83%)	
Female	14 (17%)	7 (17%)	7 (17%)	
Age (year)	66.2 ± 11.9 [23–89] (68; 60, 72)	67.9 ± 10.6 [36–89] (68; 60, 74)	64.6 ± 12.9 [23–86] (67; 60, 72)	0.233
Diagnosis of HCC				**0.013**
Biopsy	69 (84%)	39 (95%)	30 (73%)	
Surgery	13 (16%)	2 (5%)	11 (27%)	
Treatment of HCC				**0.014**
Surgery	13 (16%)	2 (5%)	11 (27%)	
RFA	31 (38%)	26 (63%)	15 (37%)	
TACE	25 (30%)	12 (29%)	13 (32%)	
RFA + TACE	1 (1%)	0 (0%)	1 (2%)	
Other*	2 (2%)	1 (2%)	1 (2%)	

Note. Qualitative variables are expressed as raw numbers; numbers in parentheses are percentages. Quantitative variables are expressed as means ± standard deviations (SD); numbers in brackets are ranges; numbers in parentheses are medians followed by first (Q1) and third (Q3) quartiles. Bold indicates significant differences. HCC indicates hepatocellular carcinoma; NASH indicates non-alcoholic steatohepatitis; RFA indicates radiofrequency ablation; TACE indicates transcatheter arterial chemoembolization.
* Sorafenib or Nexavar

Table 3. Comparison of MRI findings of hepatocellular carcinomas in 41 patients with NASH and 41 patients with virus-induced chronic liver disease

Quantitative variables	NASH (n = 41)	Virus (n = 41)	*P* value
Tumor longest axis (mm)	30.3 ± 20.9 [9–95] (23; 15, 36)	38.0 ± 26.3 [10–106] (28; 19, 56)	0.121
Tumor signal drop * (%)	11.8 ± 18.5 [0–78] (5; 0, 78)	6.0 ± 9.7 [0–39] (2; 0, 7)	0.464
ADC value ($\times 10^{-3}$ mm^2/sec)	975 ± 257 [456–1625] (995; 777, 1146)	1048 ± 253 [333–1633] (1045; 859, 1289)	0.197
Qualitative variables			
Right liver location	31 (76%)	26 (63%)	0.337
Diameter ≥ 20 mm	25 (61%)	26 (63%)	1.000
Arterial phase hyperenhancement	38 (93%)	40 (98%)	0.616
Wash out	26 (63%)	34 (83%)	0.080
Corona sign	9 (22%)	3 (7%)	0.058
Tumor fat content ǂ	22 (54%)	26 (63%)	0.502
Visibility on T1-weighted images	29 (71%)	23 (56%)	0.252
Visibility on T2-weighted images	35 (85%)	36 (88%)	1.000
Tumor capsule	28 (68%)	25 (61%)	0.488
Portal vein invasion	5 (12%)	10 (24%)	0.253
Extrahepatic metastasis	0 (0%)	0 (0%)	1.000
Li-RADS category			0.303
3	6 (15%)	3 (7%)	
4	9 (22%)	5 (12%)	
5	26 (63%)	33 (80%)	

Note. Data are given on a per lesion basis. Quantitative variables are expressed as means ± standard deviations; numbers in brackets are ranges; numbers in parentheses are medians followed by first (Q1) and third (Q3) quartiles. Qualitative variables are expressed as raw numbers; numbers in parentheses are proportions followed by percentages.

*Tumor signal drop was calculated as (tumor signal on in-phase image minus tumor signal on out-of-phase image)/tumor signal on in-phase image and expressed in %.

ǂ Tumor fat content was considered present when tumor signal drop was > 0%

ADC indicates apparent diffusion coefficient. NASH indicates non-alcoholic steatohepatitis.

Table 4. Distribution of LI-RADS v2018 major criteria in total and by underlying hepatic disease, Kappa statistic and inter reader agreement for LI-RADS major criteria and LI-RADS categorization in total and by underlying hepatic disease

Criteria	Reader 1	Reader 2	Kappa (95% CI)
Arterial phase hyperenhancement			
NASH	37 (90%)	36 (88%)	0.626 (0.239-1) *
Virus	40 (98%)	39 (95%)	0.655 (0.029-1) *
Total	77 (94%)	75 (91%)	0.641 (0.317-0.965) *
***P* value†**	0.359	0.432	
Portal venous or delayed phase wash out			
NASH	26 (63%)	28 (68%)	0.790 (0.594-0.985) *
Virus	34 (83%)	34 (83%)	0.755 (0.493-1) *
Total	60 (73%)	62 (76%)	0.786 (0.635-0.937) *
***P* value†**	0.080	0.198	
Tumor capsule			
NASH	25 (61%)	31 (76%)	0.367 (0.062-0.973) *
Virus	27 (66%)	28 (68%)	0.675 (0.438-0.913) *
Total	52 (63%)	59 (72%)	0.527 (0.331-0.723) *
***P* value†**	0.819	0.624	
Diameter ≥ 20 mm			
NASH	25 (61%)	25 (61%)	0.799 (0.612-0.986) *
Virus	26 (63%)	31 (76%)	0.648 (0.392-0.903) *
Total	51 (62%)	56 (68%)	0.733 (0.579-0.888) *
***P* value†**	0.820	0.235	
Li-RADS category			
NASH			0.802 ‡
3	7 (17%)	6 (15%)	
4	10 (24%)	8 (20%)	
5	24 (59%)	27 (66%)	
Virus			0.720 ‡
3	3 (7%)	3 (7%)	
4	4 (10%)	5 (12%)	
5	34 (80%)	33 (80%)	

Note. *Kappa test for agreement between readers for the presence of individual major criterion; † Fisher exact test for comparison between NASH and virus groups for each criterion and each reader. ‡ Weighted kappa test
NASH indicates non-alcoholic steatohepatitis